

Constraining eV-scale axion-like particle dark matter: insights from the M87 Galaxy

Arpan Kar,^a Surov Roy,^b Pratick Sarkar^b

^aLaboratoire de Physique Théorique et Hautes Énergies (LPTHE), CNRS & Sorbonne Université, 4 Place Jussieu, Paris, France

^bSchool of Physical Sciences, Indian Association for the Cultivation of Science, 2A & 2B Raja S.C Mullick Road, Kolkata-700032, India

E-mail: arpankarphys@gmail.com, tpsr@iacs.res.in, spsps2523@iacs.res.in

Abstract. Axion-like particles (ALPs) can account for the observed dark matter (DM) of the Universe and if their masses are at the eV scale, they can decay into infrared, optical and ultraviolet photons with a decay lifetime larger than the age of the Universe. We analyze multi-wavelength data obtained from the central region of Messier 87 (M87) galaxy by several telescopes, such as, Swift, Astrosat, Kanata, Spitzer and International Ultraviolet Explorer in the infrared to ultraviolet frequencies ($\sim 2 \times 10^{14}$ Hz – 3×10^{15} Hz), to constrain the narrow emission lines indicative of the eV scale ALP DM decay. We derive constraints on the ALP coupling to two photons ($g_{a\gamma\gamma}$) for ALP mass range $2 \text{ eV} \lesssim m_a \lesssim 20 \text{ eV}$, assuming ALPs form the DM in the M87 halo. We find that our bounds on ALP-two-photon coupling can become stronger than the existing ones by an order of magnitude in the ALP mass range $8 \text{ eV} \lesssim m_a \lesssim 20 \text{ eV}$.

Contents

1	Introduction	1
2	ALP DM decay signal	2
3	Observations and Data	5
4	Methodology & Results	5
4.1	Conservative approach	5
4.2	χ^2 fit constraints	7
4.2.1	Constraints from standard background	7
4.2.2	Constraints from fitted background	8
5	Conclusion	9
A	Summary of observational data in the IR-Optical-UV range	10

1 Introduction

Numerous astrophysical and cosmological observations firmly support the existence of DM, a non-baryonic, minimally interacting, cold matter component that provides about 25% of the energy density of our universe [1]. However, the microscopic features of DM are still unknown. Extensive efforts in its search suggest that DM resides in the form of new, unknown particles.

Quantum Chromodynamics (QCD) presents a fundamental challenge known as the Strong Charge-Parity (CP) problem, with axions emerging as a potential solution to this issue[2–9]. The non-observation of the neutron electric dipole moment[10] constrains the CP- violating θ - parameter to be surprisingly small, $|\theta| \leq 10^{-10}$, while its value could generically be $\mathcal{O}(1)$. A most promising solution to this strong CP problem is to introduce a new global U(1) symmetry which spontaneously breaks at some high-energy scale through the Peccei-Quinn mechanism to produce a pseudo-Nambu-Goldstone boson, known as the axion. Despite the small mass, the axions can be produced non-thermally in the early universe and are stable in cosmological time scales and can contribute substantially to the current fraction of the energy density of the Universe in the form of cold DM [11–17]. The QCD axion couples to Standard Model photons via electromagnetic anomaly and the coupling, $g_{a\gamma\gamma}$, varies linearly with the axion mass m_a . On the other hand, axion-like particles (ALPs), which possess properties similar to the QCD axion, are, however, more generic in the sense that they do not exhibit a direct one-to-one relationship between their mass and the photon coupling $g_{a\gamma\gamma}$. ALPs which naturally arise in low-energy effective theories from higher-dimensional theories [18–21] can be a potential candidate for the observed DM of the Universe. Thus, beyond the well-motivated QCD axion, it is also intriguing to explore the whole parameter space of ALPs.

Due to its couplings to photons, ALPs can decay into two photons, although the decay rate should be slow enough so that they are stable on the cosmological time scale to explain the observed DM. Astronomical telescopes can provide a powerful means of searching for signals from such ALP DM decay. The decay of ALP DM particle inside a DM dense

region such as a galactic DM halo can produce a distinctive monochromatic emission line that can be distinguished from astrophysical backgrounds. Over the years, searches for these emission lines have spanned a broad range of frequencies, from radio waves to X-rays [22–29]. In particular, if the mass m_a of the ALP particles is on the order of electronvolts (eV) then their decay would produce photons in the infrared, optical, and ultraviolet bands. In this context, rigorous spectroscopic searches have been performed in the infrared to optical frequency bands [23, 30–36] which impose constraints on the $g_{a\gamma\gamma} - m_a$ plane for ALPs, further encouraging the exploration of ALPs at the eV scale. Until recently, no searches had been conducted in the far-ultraviolet band, with the exception of a very recent study [37].

In this study, we constrain the line emission from the decay of eV scale ALP DM using the optical-ultraviolet bands in spectroscopic data collected by the Neil Gehrels Swift Observatory (which has been operational for 19 years). Its Ultraviolet/Optical Telescope (UVOT) is designed to capture optical and UV emissions from astrophysical sources. Additionally, we utilized data from the Kanata Telescope at the Hiroshima Astrophysical Science Center, which operates in the near-infrared and optical bands [38]. We also explored the near-UV and visible bands using the UV Imaging Telescope (UVIT) onboard the Astrosat mission, which features dedicated near-UV, visible, and far-UV channels [39, 40]. This work focuses on observations of the central region of Messier 87 (M87) galaxy, a DM-rich environment. In such regions, decay of ALP DM particles into two photons could lead to strong emission lines, non-observation of which by current telescopes targeting at the central part of M87 put constraint on the ALP-photon coupling. Also, the recent imaging of M87* [41–47], the supermassive black hole (SMBH) at the center of M87 galaxy, provides an unprecedented opportunity to probe phenomena beyond the Standard Model [48–50]. Two major Multi Wavelength EHT campaigns (MWL2017 [51] and MWL2018 [52]), conducted by the EHT Multi-wavelength Science Working Group (MWL WG), analyzed multi-band data from millimeter waves to TeV γ -rays for the central region of M87 galaxy. This study leverages data from the 2018 campaign (MWL2018) (with a focus on the ultraviolet and optical bands) as well as the data from previous observations [53–59] by Spitzer and International Ultraviolet Explorer focused towards M87 center in the infrared-ultraviolet band to constrain the decay of eV scale ALP DM.

This paper is organized as follows: section 2 describes the computation of the ALP DM decay signal; section 3 introduces the observational dataset; section 4 details the methodology used in our analysis and the obtained results; finally in section 5 we conclude.

2 ALP DM decay signal

In this work, we look for infrared-optical-ultraviolet emission lines from ALP DM decay ¹. The ALP can decay to two photons via the interaction

$$\mathcal{L} = -\frac{1}{4}g_{a\gamma\gamma}aF_{\mu\nu}\tilde{F}^{\mu\nu} \quad (2.1)$$

where a represents the ALP field, $F_{\mu\nu}$ and $\tilde{F}^{\mu\nu}$ denote the electromagnetic field strength tensor and its dual, respectively, and $g_{a\gamma\gamma}$ is the ALP-photon coupling. The ALP decay rate is given by:

$$\Gamma_a = \frac{g_{a\gamma\gamma}^2 m_a^3}{64\pi} \quad (2.2)$$

¹Our study, however is sensitive to any DM candidate which produces narrow emission signals.

where m_a is the ALP mass. Note that the lifetime ($1/\Gamma_a$) should be larger than the age of the universe so that the ALP can explain the observed DM density of the Universe.

The photon flux density, i.e., the radiated power per unit area per unit frequency, from the decay of ALP DM is given by [60]:

$$S_{decay} = \frac{\Gamma_a}{4\pi\Delta\nu} \int d\theta 2\pi \sin\theta \int_{l.o.s} dl \rho_a(r(l,\theta)). \quad (2.3)$$

Here $\Delta\nu$ is the width of the produced photon line, given by $\Delta\nu = \nu_c \sigma_d$, where ν_c is the central frequency ($= m_a/4\pi$) of the photon line and σ_d is the velocity dispersion of DM particles within the DM halo. The decay signal will follow a Gaussian distribution, centered around the flux S_{decay} as the peak value, with $\Delta\nu$ representing the spread of the signal. We study ALP DM decay signal from the central region of the M87 galaxy which hosts a super massive black hole (SMBH). Around the SMBH the velocity dispersion of DM is given by $\sqrt{\frac{2G_N M_{BH}}{r}} c$ [61], where G_N is the gravitational constant, c is the speed of light and M_{BH} is the black hole mass which for the central SMBH in M87 is $M_{BH} \simeq 6.5 \times 10^9 M_\odot$ [52]. Additionally, there is also an outer halo component of the DM velocity dispersion which is of the order of $10^{-3}c$. The integral in Eq. 2.3 is performed over the line of sight (l.o.s) l between the emitting object and the location of Earth and the angle θ covered by the observing telescope. The radial distance from the center of M87 galaxy $r(l, \theta)$ is given by $r = \sqrt{l^2 + d^2 - 2ld \cos\theta}$, where d is the distance of the M87 center from Earth. In order to take into account the effect of absorption of the DM induced photons, we remove the contribution from the central region $r \lesssim 100R_s$ (with R_s being the Swartzchild radius of the SMBH) from Eq. 2.3, where the absorption can be stronger [52].

In Eq. 2.3, $\rho_a(r)$ describes the DM mass density distribution in the inner region of M87 galaxy. For $\rho_a(r)$ we adopt the NFW profile [62, 63],

$$\rho_{\text{NFW}}(r) = \frac{\rho_0}{(r/r_0)(1 + r/r_0)^2}, \quad (2.4)$$

with ρ_0 and r_0 are the scale density and scale radius, respectively.

The parameters for the M87 galaxy within the Virgo Cluster are: $\rho_0 = 6.96 \times 10^5 M_\odot/kpc^3$, $r_0 = 403.8kpc$, spread of the virial radius of the DM halo is approximately 1.7 Mpc and distance from the earth $d = 17.2$ Mpc [63]. Additionally, we will also consider the NFW DM profile from [64] with different profile parameters.

In the bottom panel of Fig. 1, the blue line shows an example of the ALP DM signal from the central region of M87. Such a signal is estimated with the DM profile parameters mentioned above. The ALP mass is considered to be $m_a = 9.51$ eV, with the value of $g_{a\gamma\gamma}$ set to $1.52 \times 10^{-11} \text{ GeV}^{-1}$ which corresponds to the existing bound on the coupling at this mass. This m_a produces an observed frequency of $\nu = 1.15 \times 10^{15}$ Hz. The angular width of observation is taken to be the one that corresponds to the resolution used at that frequency.

In the literature, the DM density near the center of galaxies (such as M87) is often described by a spike profile (due to the presence of a SMBH at the center) [64–67]. However, for this study, we only adopt the canonical NFW profile. We checked that our DM decay signal remains almost unaffected even when a spike profile is superimposed on the NFW profile.

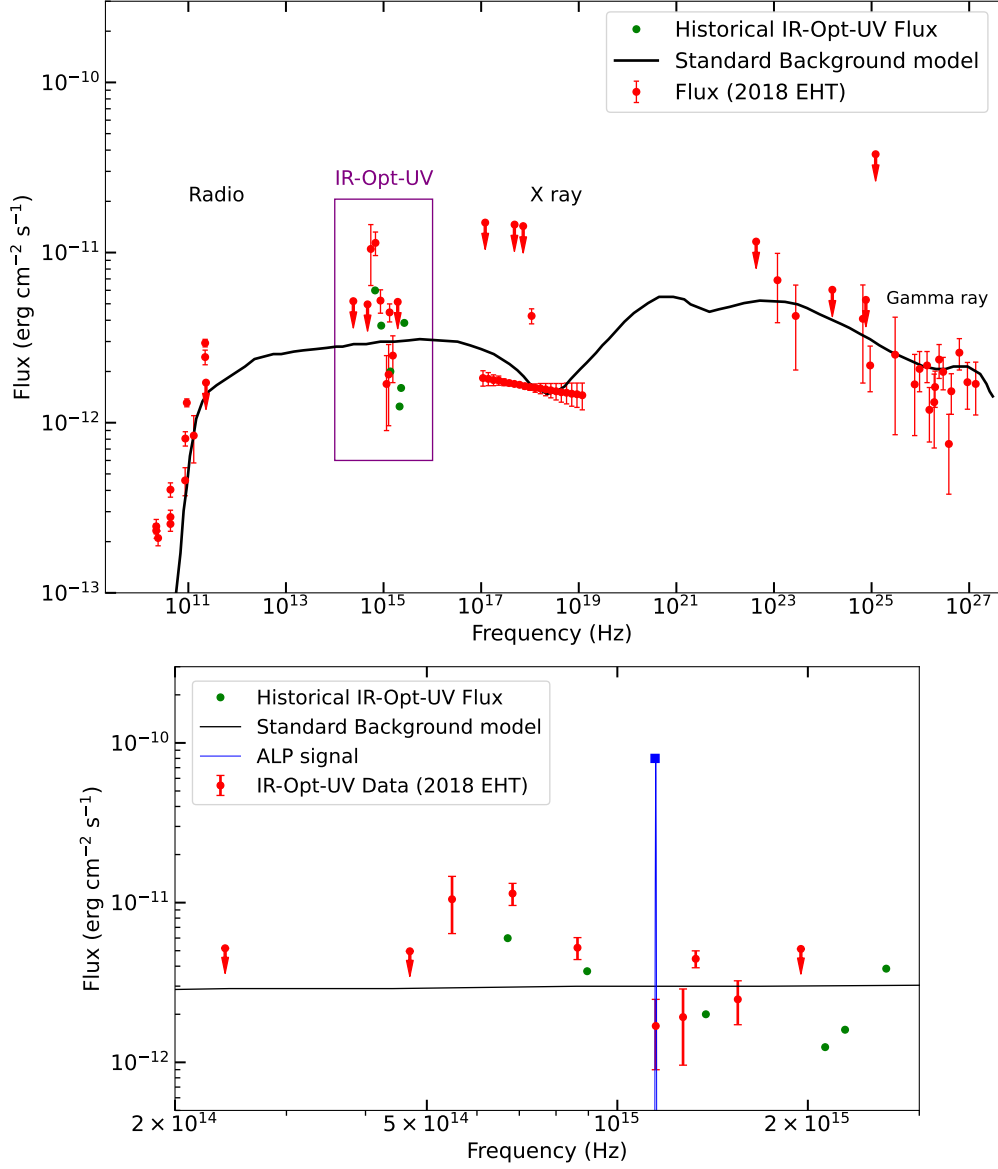


Figure 1. The observed broadband SED of M87, measured during the April 2018 Event Horizon Telescope (EHT) campaign using various instruments, are shown in red points. The measurements, represented by red points with error bars, indicate observed flux with experimental uncertainties, while red downward arrows denote upper limits on flux estimates. The black line depicts the best-fit model (modified model A) applied to the entire dataset, as mentioned in [52]. Additionally, the green dots represent the historical data in the IR-optical-UV frequency range from earlier observations of M87, compiled from studies such as [53–59, 68–70]. *Bottom panel:* The IR-optical-UV frequency range which is highlighted by a box in the top panel, is shown in the bottom panel as a zoomed-in view. Here the ALP DM decay signal from M87 is shown by the blue line. Such a signal is estimated for $m_a = 9.51$ eV with the value of $g_{a\gamma\gamma}$ set to the corresponding existing bound, i.e., $g_{a\gamma\gamma} = 1.52 \times 10^{-11} \text{ GeV}^{-1}$.

3 Observations and Data

Our analysis emphasizes the infrared, optical, and UV observations within M87’s broad spectrum, from which we can constrain the ALP-photon coupling.

The dataset utilized in this study, is drawn from the campaign paper [52] which details the second multi-wavelength observational campaign on M87 by the MWL WG. The measured spectral energy distribution (SED) data for M87 can be accessed via the data archive at [71]. The MWL WG collaboration used state-of-the-art data reduction techniques to publish this dataset, covering an electromagnetic flux range from 10^{10} to 10^{27} Hz. These 2018 flux measurements are represented as red points in Fig. 1.

During this observational campaign, in the IR-Optical-UV region, four telescopes have been utilized for observations. The Swift UV-Optical Telescope (UVOT) observed the M87 galaxy with an angular resolution of $3''$, collecting data over a wavelength range of approximately 192–547 nm. The Kanata Telescope contributed data up to an upper flux limit at 634.5 nm and 1250 nm within a $10'' \times 10''$ field of view. The UV Imaging Telescope (UVIT), part of the AstroSat mission, provided observations with two telescopes: one focused on the near-UV (2000–3000 Å) and visible (3200–5500 Å) bands, and the other on the far-UV (1300–1800 Å), offering upper flux limits with a large $300''$ field of view. We will be using single data point obtained in the near-UV channel. The Hubble Space Telescope (HST), operating in the UV-optical range, measured the flux at a central wavelength of 236 nm but with a relatively small resolution of $0.1''$. In total, there are 10 data points in the IR-Optical-UV bands, with seven having associated error bars for flux estimation.

The M87 SED are also informed by a series of earlier datasets. These older datasets include core emission measurements (ranging from millimeter to X-ray frequencies) [53–59, 68–70], MOJAVE VLBA observations at radio frequencies [72], Chandra X-ray data from 2009 [73], Fermi-LAT data [74], HESS data [75], VERITAS data [76], and MAGIC data [77]. The infrared-optical-UV frequency range of this older dataset, referred to in this paper as “Historical data”, is displayed as green points in Fig. 1.

The details of these observations are summarized in appendix A.

4 Methodology & Results

The contributions of the ALP DM signal at the observed frequencies (i.e., in IR, Optical and UV) are estimated within the angular resolution of the telescopes, focused towards the center of M87. The angular resolution is determined by the specifications of each telescope for specific frequency windows across the electromagnetic spectrum. Comparing the ALP signal with the observed data, we derive bounds on the ALP-two-photon coupling $g_{a\gamma\gamma}$. In this work, we take two different approaches to derive these bounds on $g_{a\gamma\gamma}$. Below, we describe each approach and the corresponding constraints obtained in each case.

4.1 Conservative approach

This approach, serving as a conservative estimate, asserts that the DM signal must not exceed the observed data in any of the frequency bins that we are considering. This approach does not involve any modeling of the background, which makes it conservative in that regard. There are total ten data points (including observed data with error bars as well as upper-limits) from the EHT2018 in the IR-Optical-UV range. In addition, the historical dataset has six observed data points. For details, see Fig. 1 and Appendix A. For a given ALP mass m_a

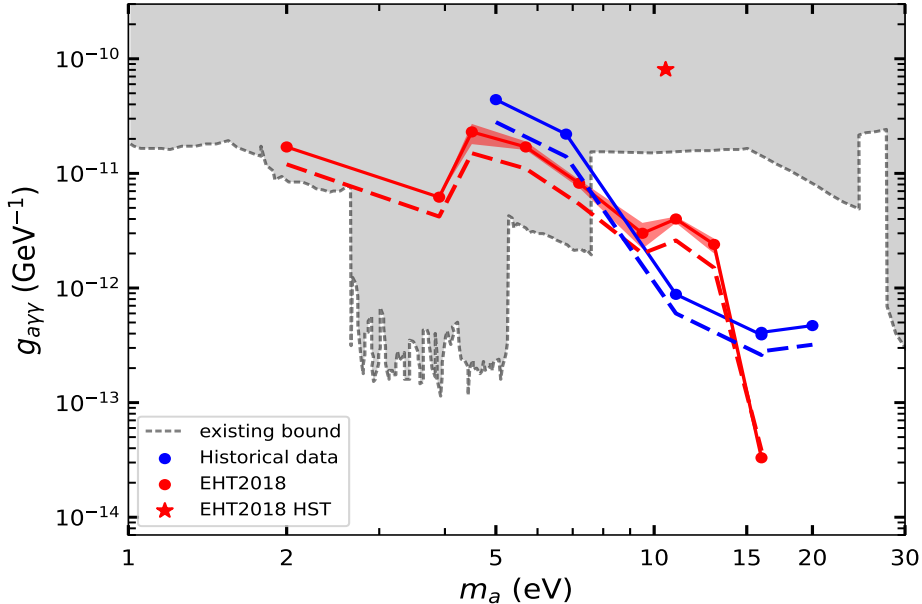


Figure 2. Constraints on the axion photon coupling $g_{a\gamma\gamma}$ considering the conservative approach (described in Section 4.1), is shown in the figure. The red and blue lines correspond to the 2018 observational campaign and the historical observational dataset of M87, respectively. The band around the constraint shown by the red solid line demonstrates the observational uncertainty in the data at relevant frequencies (see Table 1). The single red star corresponds to the EHT(2018) HST observed data point. The dashed red and blue lines are the constraints obtained for an alternative DM profile discussed in the text. The gray shaded region indicates the strongest existing bound in the $m_a - g_{a\gamma\gamma}$ plane [24, 28, 30, 31, 34, 35, 78].

that corresponds to any of these observed frequencies, we obtained bound on $g_{a\gamma\gamma}$ requiring that the photon signal arising from the ALP decay (given in Eq. 2.3) does not exceed the observed data. The bounds obtained with this approach are shown in the $m_a - g_{a\gamma\gamma}$ plane in Fig. 2.

As can be seen from Fig. 2, we are able to put constraints in the mass window (2-16) eV for the EHT(2018) dataset (shown by red solid and dashed curves) and in the mass window (5-20) eV for the historical dataset (blue solid and dashed curves). The constraints shown by the solid red and blue lines correspond to the NFW DM profile with the parameters obtained from [63] as mentioned in Section 2. In addition, we also show that the constraints (by the dashed red and blue lines) correspond to a NFW DM profile, but with different parameters: $\rho_0 = 6.5 \times 10^7 M_\odot/kpc^3$, $r_0 = 20kpc$ (obtained from [64]). The rest of our discussion will be based on the former NFW profile parameters.

We compare our bounds with the existing constraints (obtained from [24, 28, 30, 31, 34, 35, 78])² that are shown as the gray-shaded region in the $m_a - g_{a\gamma\gamma}$ plane. We find that, our constraints can surpass the existing bounds on $g_{a\gamma\gamma}$ by an order of magnitude for the ALP mass range $8eV \lesssim m_a \lesssim 20eV$. Only for the single data from the HST observation, the

²The existing constraints are estimated from the data files corresponding to the relevant mass range, available on the website [79]. The strongest limit on the coupling was identified and used as the upper boundary of the allowed parameter space.

constraint on the coupling (shown as red star) falls inside the existing bound due to the weak sensitivity of HST towards DM decay signal, owing to its much smaller angular resolution (see Table 1).

4.2 χ^2 fit constraints

In the second approach, the bounds on the coupling are derived considering a background fit model. We refer to this approach here as the χ^2 fit constraints. Based on the astrophysical background model that describes the observed data over the whole frequency range, we will incorporate photon emissions resulting from ALP decay to constrain the parameter space.

4.2.1 Constraints from standard background

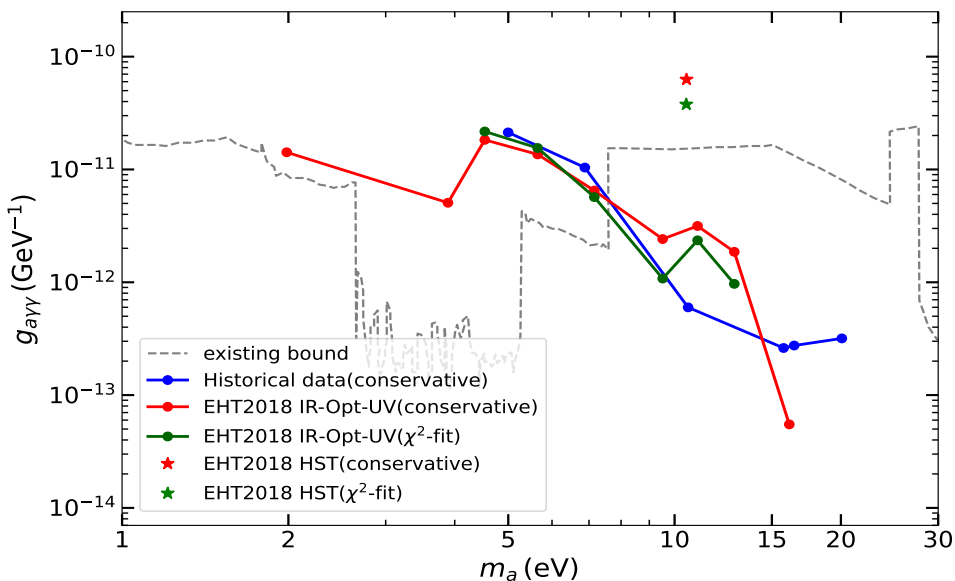


Figure 3. Upper-limit on $g_{a\gamma\gamma}$ obtained (at 95% C.L.) considering a background model (modified model A from [52]) is shown by the green line (see Section 4.2.1). The result corresponds to the HST data is shown separately by green star. For comparison, constraints derived using the conservative approach are also presented: the red line corresponds to the EHT (2018) dataset, and the blue line corresponds to the historical dataset.

Given that the observed data are unevenly distributed across a wide frequency range, it is practical to fit a single model that accounts for the entire spectrum uniformly. A comprehensive review of astrophysical models, including their parameters, is provided in MWL2018 [52]. In this analysis, we adopt the modified Model A from [52] as the standard astrophysical background.

Now to estimate the coupling $g_{a\gamma\gamma}$, we perform a χ^2 analysis where χ^2 is defined as:

$$\chi^2(m_a, g_{a\gamma\gamma}) = \sum_{i=1}^N \left(\frac{S_{\text{th}}^i - S_{\text{obs}}^i}{\sigma_{\text{obs}}^i} \right)^2. \quad (4.1)$$

Here, S_{th}^i is the theoretical flux in the i -th frequency bin, computed as $S_{\text{th}}^i = S_{\text{signal}}^i + S_{\text{background}}^i$. The S_{signal}^i is the ALP DM signal computed using Eq. 2.3, and $S_{\text{background}}^i$

is derived from the modified Model A. S_{obs}^i is the observed flux, and σ_{obs}^i represents the associated observational uncertainty.

Here the summation runs over all frequency bins. For a fixed DM mass m_a , the function χ^2 depends only on $g_{a\gamma\gamma}$. The significance of a signal from ALP decay can then be computed using:

$$\Delta\chi^2 = \chi^2(g_{a\gamma\gamma}) - \chi_{\text{min}}^2. \quad (4.2)$$

For a 95% confidence level (C.L.) and one degree of freedom, $\Delta\chi^2 = 2.71$.

The quantity χ_{min}^2 , the minimum value of χ^2 , corresponds to the best-fitted background model [52] without any signal (that is, for a vanishing axion-photon coupling). Taking into account the EHT(2018) whole dataset we first obtain χ_{min}^2 , then we add the DM signal in the frequency bin corresponding to m_a with varying $g_{a\gamma\gamma}$ and estimate the constraint on it within 95% C.L.

The constraint on $g_{a\gamma\gamma}$ obtained in this method is shown in Fig. 3 by the green solid line, along with the conservative limit discussed in Section 4.1 (shown as red solid line) for comparison. The χ^2 -analysis of the entire dataset gives constraints in the mass range $4.3\text{ eV} \lesssim m_a \lesssim 12.8\text{ eV}$, of which the mass range $8\text{ eV} \lesssim m_a \lesssim 12.8\text{ eV}$ have almost an order of magnitude stronger constraints compared to the existing bounds. The green star demonstrates the limit on the coupling for the frequency bin corresponding to HST data.

4.2.2 Constraints from fitted background

We also performed a fit to the infrared-optical-UV data points using a higher-degree polynomial model, as shown on the top panel of Fig. 4. Due to the irregular distribution of these data points relative to the standard background, a conventional power-law model does not provide a good fit in this frequency range. Instead, we identified the best-fit curve for these 7 data points using a polynomial model. Based on this fitted model, the constraints on the $m_a - g_{a\gamma\gamma}$ parameter space are obtained.

The fitted model is expressed as:

$$F(\nu) = a_0 + a_1(\nu/\nu_0) + a_2(\nu/\nu_0)^2 + a_3(\nu/\nu_0)^3 + a_4(\nu/\nu_0)^4 \quad (4.3)$$

where ν_0 is a reference frequency chosen to be 10^{15} Hz. The fit yielded a $\chi^2/d.o.f = 0.98$ with the best-fit parameters: $a_0 = -2.05 \times 10^{-10} \text{ erg cm}^{-2} \text{ s}^{-1}$, $a_1 = 9.92 \times 10^{-10} \text{ erg cm}^{-2} \text{ s}^{-1}$, $a_2 = -1.605 \times 10^{-9} \text{ erg cm}^{-2} \text{ s}^{-1}$, $a_3 = 1.08 \times 10^{-9} \text{ erg cm}^{-2} \text{ s}^{-1}$ and $a_4 = -2.56 \times 10^{-10} \text{ erg cm}^{-2} \text{ s}^{-1}$. This fitted model was then treated as the background for further analysis.

Using this background model, the same χ^2 -fit method (discussed in Section 4.2.1 with a focus on the infrared-optical-UV part of the data) was applied to constrain the coupling $g_{a\gamma\gamma}$ for a given m_a . In the bottom panel of Fig. 4, the blue dashed line represents the 95% C.L. upper limit in the $g_{a\gamma\gamma} - m_a$ plane for the fitted background model. Additionally, the solid cyan line shows the constraints if the fitted model flux is directly interpreted as the upper bound of the ALP signal (i.e., without performing any χ^2 analysis with the signal). For comparison, the conservative limit (discussed in Section 4.1) as well as constraints obtained using the modified model A as background (discussed in Section 4.2.1) are also shown in the figure.

As shown in the figure, the fitted model provides slightly stronger constraints at the lower end of the mass range, whereas the standard background (the modified model A from [52]) yields tighter constraints at the higher mass range.

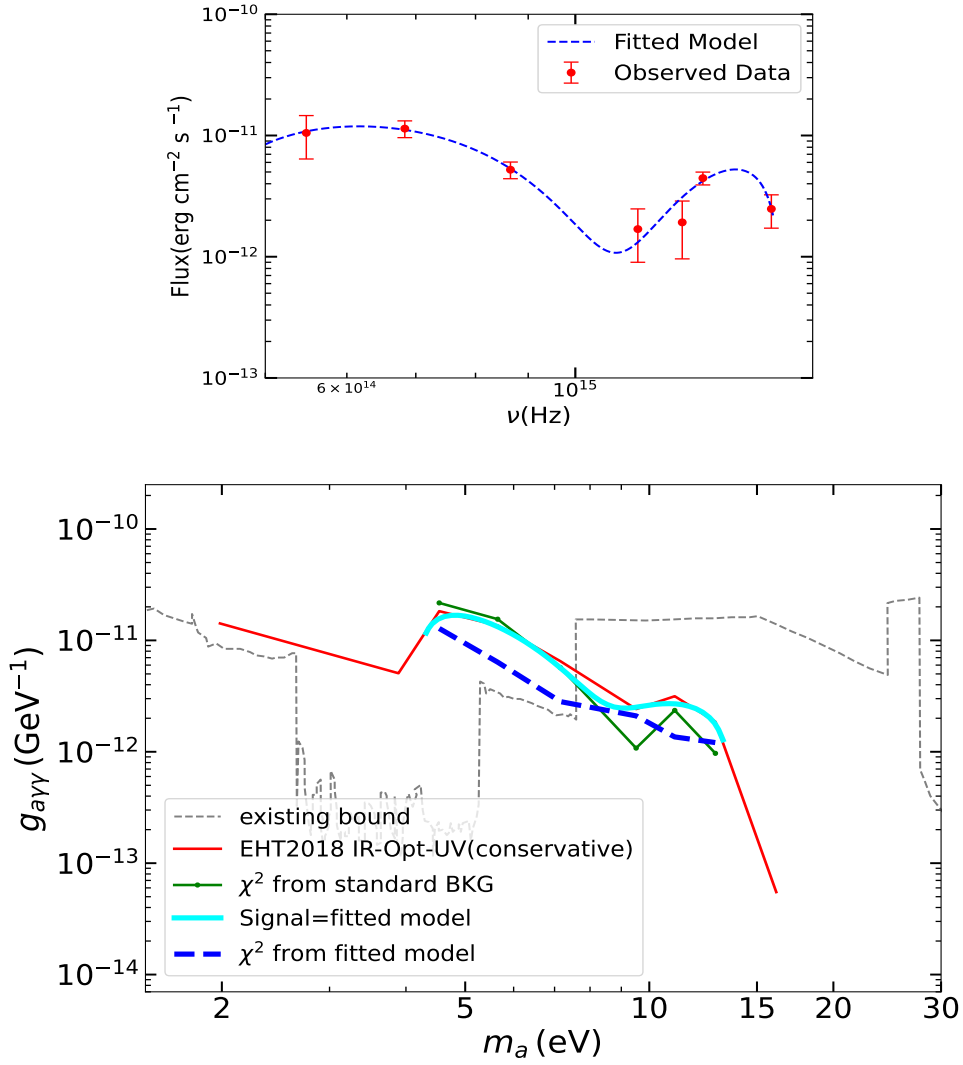


Figure 4. *Top panel:* The blue dashed line represents the fit to the 2018 (EHT) data in the IR-Opt-UV frequency range (see Section 4.2.2 for details). *Bottom panel:* The dashed blue line shows the constraint on $g_{a\gamma\gamma}$ derived (at 95% C.L.) using the fitted background model shown in the top panel. The solid cyan line corresponds to the constraint obtained assuming the fitted background model as the upper limit for the ALP DM decay signal. Constraints obtained using the standard background (BKG) model and the conservative approach are also presented for comparison.

5 Conclusion

Due to its coupling with the SM photon, an axion-like particle (ALP) can decay into two photons. Assuming that ALPs account for the entire observed cold DM abundance of the Universe, their decay near the central region of galaxies, which is expected to be DM-rich, can give rise to observable line emission signals.

Based on this, in this work we have constrained the ALP-two-photon coupling $g_{a\gamma\gamma}$ of the ALP DM with mass in the range $2\text{eV} \lesssim m_a \lesssim 20\text{eV}$, using the observation of M87 galaxy in infrared, optical and ultraviolet emission. For this we have used the dataset of the central region of M87, obtained by the EHT Multi-wavelength Science Working Group

(MWL WG) during their 2018 observational campaign, as well as the old dataset for the same region collected over the years. The recent data were collected by Swift-UVOT, HST, Astrosat-UVIT and Kanata telescope. The historical data were collected by the spitzer space telescope and International Ultraviolet Explorer. Based on such data we exclude $g_{a\gamma\gamma} \gtrsim 10^{-11} \text{ GeV}^{-1} - 10^{-13} \text{ GeV}^{-1}$ in the above-mentioned mass window. Fig. 2 shows the results obtained in a conservative approach without assuming any background model. The χ^2 -fit analysis make the constraints stronger in the mass range $4 \text{ eV} \lesssim m_a \lesssim 13 \text{ eV}$ which is presented in Fig. 3 and Fig. 4. The better constraints are obtained by Swift-UVOT, Astrosat-UVIT and Kanata telescope due to their wide field observations. Such constraints surpass the existing bounds on $g_{a\gamma\gamma}$ by an order of magnitude in the mass range $8 \text{ eV} \lesssim m_a \lesssim 20 \text{ eV}$. On the other hand, HST has a low sensitivity for the ALP DM decay signal due to its small angular resolution.

For the DM density distribution near the central region of M87 we use a standard NFW profile. It is also possible to model this density distribution in the form of a DM spike, but our results for decaying ALP DM remain unchanged due to this.

The constraints can be improved through increasing the sensitivity of the observing telescopes and onboard spectrometers. One can improve the bounds by enhancing the data reduction maneuvers from the Swift-UVOT telescope in the upcoming future. Future telescopes like the LUVOIR and on-board spectrograph LUMOS [80] will be able to obtain higher sensitivity for the Infrared-optical-UV emission lines, and thus will be able to further improve the constraints on the ALP DM decay. UVEX [81] can serve as a future telescope in the UV frequency range.

Acknowledgements

AK acknowledges the hospitality of the Institut d’Astrophysique de Paris (IAP) where part of this work was done. PS receives support from the University Grants Commission, Government of India, through a Senior Research Fellowship.

A Summary of observational data in the IR-Optical-UV range

The data central to this study, focusing on infrared, optical, and ultraviolet emissions from the central region of the M87 galaxy, are summarized in the table 1. The multi wavelength dataset of M87 can be obtained from the data table of the MWL WG published article [52]. The table 1 represents the working frequencies of the telescopes along with their resolutions and measured fluxes. On the other hand, we also incorporated a historical dataset, collected over several years [53–59, 68–70], which is represented by green dots in the Fig. 1 (not shown in a table). The historical data in the infrared-optical range were collected by spitzer space telescope with telescopic resolution in the ballpark of $\simeq 1''$ and in the ultraviolet region the data were obtained by the International Ultraviolet Explorer (IUE) with a resolution of $\simeq 10''$.

ν (Hz)	Angular Scale [μ]	νS_ν (erg cm ⁻² s ⁻¹)	Telescope/Observatory
2.4×10^{14}	10.0	$< 5.18 \times 10^{-12}$	Kanata
4.7×10^{14}	10.0	$< 4.96 \times 10^{-12}$	Kanata
5.48×10^{14}	3.0	$1.05 \pm 0.41 \times 10^{-11}$	Swift-UVOT
6.83×10^{14}	3.0	$(1.14 \pm 0.18) \times 10^{-11}$	Swift-UVOT
8.65×10^{14}	3.0	$(5.22 \pm 0.82) \times 10^{-12}$	Swift-UVOT
1.15×10^{15}	3.0	$(1.69 \pm 0.79) \times 10^{-12}$	Swift-UVOT
1.27×10^{15}	0.1	$(1.92 \pm 0.96) \times 10^{-12}$	HST
1.33×10^{15}	3.0	$(4.45 \pm 0.54) \times 10^{-12}$	Swift-UVOT
1.55×10^{15}	3.0	$(2.48 \pm 0.76) \times 10^{-12}$	Swift-UVOT
1.95×10^{15}	300.0	$< 5.13 \times 10^{-12}$	AstroSat-UVIT

Table 1. This table summarizes the observed data for infrared, optical and ultraviolet emissions from the central region of the M87 galaxy. These data were gathered during 2018 campaign (by MWL WG) by various telescopes such as Swift-UVOT, Kanata, Astrosat-UVIT, HST at the frequencies listed in the first column. The angular resolutions used by different telescopes are provided in arc-seconds(μ) corresponding to their respective working frequencies. The data collected by the Swift-UVOT and HST include the experimental errors in flux measurements, while the data collected by Kanata and Astrosat-UVIT only provide upper limits on the flux.

References

- [1] PLANCK collaboration, *Planck 2018 results. VI. Cosmological parameters*, *Astron. Astrophys.* **641** (2020) A6 [[1807.06209](#)].
- [2] R.D. Peccei and H.R. Quinn, *CP Conservation in the Presence of Instantons*, *Phys. Rev. Lett.* **38** (1977) 1440.
- [3] R.D. Peccei and H.R. Quinn, *Constraints Imposed by CP Conservation in the Presence of Instantons*, *Phys. Rev. D* **16** (1977) 1791.
- [4] S. Weinberg, *A New Light Boson?*, *Phys. Rev. Lett.* **40** (1978) 223.
- [5] F. Wilczek, *Problem of Strong P and T Invariance in the Presence of Instantons*, *Phys. Rev. Lett.* **40** (1978) 279.
- [6] M.A. Shifman, A.I. Vainshtein and V.I. Zakharov, *Can Confinement Ensure Natural CP Invariance of Strong Interactions?*, *Nucl. Phys. B* **166** (1980) 493.
- [7] A.R. Zhitnitsky, *On Possible Suppression of the Axion Hadron Interactions. (In Russian)*, *Sov. J. Nucl. Phys.* **31** (1980) 260.
- [8] J.E. Kim, *Weak Interaction Singlet and Strong CP Invariance*, *Phys. Rev. Lett.* **43** (1979) 103.
- [9] M. Dine, W. Fischler and M. Srednicki, *A Simple Solution to the Strong CP Problem with a Harmless Axion*, *Phys. Lett. B* **104** (1981) 199.
- [10] J.M. Pendlebury et al., *Revised experimental upper limit on the electric dipole moment of the neutron*, *Phys. Rev. D* **92** (2015) 092003 [[1509.04411](#)].
- [11] J. Preskill, M.B. Wise and F. Wilczek, *Cosmology of the Invisible Axion*, *Phys. Lett. B* **120** (1983) 127.
- [12] L.F. Abbott and P. Sikivie, *A Cosmological Bound on the Invisible Axion*, *Phys. Lett. B* **120** (1983) 133.
- [13] M. Dine and W. Fischler, *The Not So Harmless Axion*, *Phys. Lett. B* **120** (1983) 137.

- [14] L.D. Duffy and K. van Bibber, *Axions as Dark Matter Particles*, *New J. Phys.* **11** (2009) 105008 [0904.3346].
- [15] L. Hui, J.P. Ostriker, S. Tremaine and E. Witten, *Ultralight scalars as cosmological dark matter*, *Phys. Rev. D* **95** (2017) 043541 [1610.08297].
- [16] F. Chadha-Day, J. Ellis and D.J.E. Marsh, *Axion dark matter: What is it and why now?*, *Sci. Adv.* **8** (2022) abj3618 [2105.01406].
- [17] C.B. Adams et al., *Axion Dark Matter*, in *Snowmass 2021*, 3, 2022 [2203.14923].
- [18] P. Svrcek and E. Witten, *Axions In String Theory*, *JHEP* **06** (2006) 051 [hep-th/0605206].
- [19] A. Arvanitaki, S. Dimopoulos, S. Dubovsky, N. Kaloper and J. March-Russell, *String Axiverse*, *Phys. Rev. D* **81** (2010) 123530 [0905.4720].
- [20] D. Maity, S. Roy and S. SenGupta, *Constraining the Randall-Sundrum modulus in the light of recent PVLAS data*, *Phys. Rev. D* **77** (2008) 015010 [0709.3940].
- [21] S. Haque, S. Roy and S. SenGupta, *Translating current ALP photon coupling strength bounds to the Randall-Sundrum model*, 2411.08396.
- [22] B.M. Roach, S. Rossland, K.C.Y. Ng, K. Perez, J.F. Beacom, B.W. Grefenstette et al., *Long-exposure NuSTAR constraints on decaying dark matter in the Galactic halo*, *Phys. Rev. D* **107** (2023) 023009 [2207.04572].
- [23] K. Nakayama and W. Yin, *Anisotropic cosmic optical background bound for decaying dark matter in light of the LORRI anomaly*, *Phys. Rev. D* **106** (2022) 103505 [2205.01079].
- [24] J.L. Bernal, A. Caputo, G. Sato-Polito, J. Mirocha and M. Kamionkowski, *Seeking dark matter with γ -ray attenuation*, *Phys. Rev. D* **107** (2023) 103046 [2208.13794].
- [25] S. Roy, C. Blanco, C. Dessert, A. Prabhu and T. Temim, *Sensitivity of JWST to eV-Scale Decaying Axion Dark Matter*, 2311.04987.
- [26] A. Dekker, E. Peerbooms, F. Zimmer, K.C.Y. Ng and S. Ando, *Searches for sterile neutrinos and axionlike particles from the galactic halo with erosita*, *Phys. Rev. D* **104** (2021) 023021.
- [27] H. Wang et al., *Spectroscopic search for optical emission lines from dark matter decay*, *Phys. Rev. D* **110** (2024) 103007 [2311.05476].
- [28] P. Carena, G. Lucente and E. Vitagliano, *Probing the blue axion with cosmic optical background anisotropies*, *Phys. Rev. D* **107** (2023) 083032 [2301.06560].
- [29] S. Porras-Bedmar, M. Meyer and D. Horns, *Novel bounds on decaying axionlike particle dark matter from the cosmic background*, *Phys. Rev. D* **110** (2024) 103501 [2407.10618].
- [30] D. Grin, G. Covone, J.-P. Kneib, M. Kamionkowski, A. Blain and E. Jullo, *A Telescope Search for Decaying Relic Axions*, *Phys. Rev. D* **75** (2007) 105018 [astro-ph/0611502].
- [31] M. Regis, M. Taoso, D. Vaz, J. Brinchmann, S.L. Zoutendijk, N.F. Bouché et al., *Searching for light in the darkness: Bounds on ALP dark matter with the optical MUSE-faint survey*, *Phys. Lett. B* **814** (2021) 136075 [2009.01310].
- [32] A. Caputo, A. Vittino, N. Fornengo, M. Regis and M. Taoso, *Searching for axion-like particle decay in the near-infrared background: an updated analysis*, *JCAP* **05** (2021) 046 [2012.09179].
- [33] E. Todarello, M. Regis, J. Reynoso-Cordova, M. Taoso, D. Vaz, J. Brinchmann et al., *Robust bounds on ALP dark matter from dwarf spheroidal galaxies in the optical MUSE-Faint survey*, *JCAP* **05** (2024) 043 [2307.07403].
- [34] R. Janish and E. Pinetti, *Hunting Dark Matter Lines in the Infrared Background with the James Webb Space Telescope*, 2310.15395.
- [35] W. Yin et al., *First Result for Dark Matter Search by WINERED*, 2402.07976.

- [36] M. Regis, M. Taoso and J.T. Calvo, *Searching for axion-like particles with SPHEREx*, [2412.12286](#).
- [37] E. Todarello and M. Regis, *Bounds on axions-like particles shining in the ultra-violet*, [2412.02543](#).
- [38] I.S. McLean, S.K. Ramsay and H. Takami, eds., *Ground-based and Airborne Instrumentation for Astronomy IV*, vol. 8446 of *Society of Photo-Optical Instrumentation Engineers (SPIE) Conference Series*, Sept., 2012.
- [39] S.N. Tandon, J.B. Hutchings, S.K. Ghosh, A. Subramaniam, G. Koshy, V. Girish et al., *In-orbit performance of uvit and first results*, *Journal of Astrophysics and Astronomy* **38** (2017) .
- [40] S.K. Ghosh, P. Joseph, A. Kumar, J. Postma, C.S. Stalin, A. Subramaniam et al., *In-orbit performance of UVIT over the past 5 years*, *Journal of Astrophysics and Astronomy* **42** (2021) 20 [[2012.13525](#)].
- [41] EVENT HORIZON TELESCOPE collaboration, *First M87 Event Horizon Telescope Results. II. Array and Instrumentation*, *Astrophys. J. Lett.* **875** (2019) L2 [[1906.11239](#)].
- [42] EVENT HORIZON TELESCOPE collaboration, *First M87 Event Horizon Telescope Results. III. Data Processing and Calibration*, *Astrophys. J. Lett.* **875** (2019) L3 [[1906.11240](#)].
- [43] EVENT HORIZON TELESCOPE collaboration, *First M87 Event Horizon Telescope Results. IV. Imaging the Central Supermassive Black Hole*, *Astrophys. J. Lett.* **875** (2019) L4 [[1906.11241](#)].
- [44] EVENT HORIZON TELESCOPE collaboration, *First M87 Event Horizon Telescope Results. V. Physical Origin of the Asymmetric Ring*, *Astrophys. J. Lett.* **875** (2019) L5 [[1906.11242](#)].
- [45] EVENT HORIZON TELESCOPE collaboration, *First M87 Event Horizon Telescope Results. VI. The Shadow and Mass of the Central Black Hole*, *Astrophys. J. Lett.* **875** (2019) L6 [[1906.11243](#)].
- [46] K. Akiyama et al., *First m87 event horizon telescope results. vii. polarization of the ring*, *The Astrophysical Journal Letters* **910** (2021) L12.
- [47] EVENT HORIZON TELESCOPE collaboration, *First M87 Event Horizon Telescope Results. VIII. Magnetic Field Structure near The Event Horizon*, *Astrophys. J. Lett.* **910** (2021) L13 [[2105.01173](#)].
- [48] K. Nomura, K. Saito and J. Soda, *Observing axions through photon ring dimming of black holes*, *Phys. Rev. D* **107** (2023) 123505 [[2212.03020](#)].
- [49] S. Roy, P. Sarkar, S. Sau and S. SenGupta, *Exploring axions through the photon ring of a spherically symmetric black hole*, *JCAP* **11** (2023) 099 [[2310.05908](#)].
- [50] Y. Chen, J. Shu, X. Xue, Q. Yuan and Y. Zhao, *Probing Axions with Event Horizon Telescope Polarimetric Measurements*, *Phys. Rev. Lett.* **124** (2020) 061102 [[1905.02213](#)].
- [51] EVENT HORIZON TELESCOPE, FERMI-LAT, H.E.S.S., MAGIC, VERITAS, EAVN collaboration, *Broadband Multi-wavelength Properties of M87 during the 2017 Event Horizon Telescope Campaign*, *Astrophys. J. Lett.* **911** (2021) L11 [[2104.06855](#)].
- [52] EVENT HORIZON TELESCOPE - MULTI-WAVELENGTH SCIENCE WORKING GROUP, EVENT HORIZON TELESCOPE, FERMI LARGE AREA TELESCOPE, H.E.S.S., MAGIC, VERITAS, EAVN, EVENT HORIZON TELESCOPE MULTI-WAVELENGTH SCIENCE collaboration, *Broadband Multi-wavelength Properties of M87 during the 2018 EHT Campaign including a Very High Energy Flaring Episode*, *Astronomy and Astrophysics* (2024) [[2404.17623](#)].
- [53] G.C. Perola and M. Tarengi, *IUE spectra of the jet and the nucleus of M 87.*, *The Astrophysics Journal* **240** (1980) 447.
- [54] J.A. Biretta, C.P. Stern and D.E. Harris, *The Radio to X-ray Spectrum of the M87 Jet and Nucleus*, *The Astronomical Journal* **101** (1991) 1632.

- [55] V. Despringre, D. Fraix-Burnet and E. Davoust, *First millimeter mapping of the jet and nucleus of M 87.*, *Astronomy and Astrophysics* **309** (1996) 375.
- [56] J.A. Biretta, W.B. Sparks and F. Macchetto, *Hubble Space Telescope Observations of Superluminal Motion in the M87 Jet*, *The Astrophysics Journal* **520** (1999) 621.
- [57] E.S. Perlman, D.E. Harris, J.A. Biretta, W.B. Sparks and F.D. Macchetto, *Month-timescale optical variability in the m87 jet*, *The Astrophysical Journal* **599** (2003) L65.
- [58] Y. Shi, G.H. Rieke, D.C. Hines, K.D. Gordon and E. Egami, *Thermal and non-thermal infrared emission from M87*, *Astrophys. J.* **655** (2007) 781 [[astro-ph/0610494](#)].
- [59] E.S. Perlman, R.E. Mason, C. Packham, N.A. Levenson, M. Elitzur, J.J. Schaefer et al., *The Mid-Infrared Emission of M87*, *Astrophys. J.* **663** (2007) 808 [[0704.1156](#)].
- [60] A. Caputo, M. Regis, M. Taoso and S.J. Witte, *Detecting the Stimulated Decay of Axions at RadioFrequencies*, *JCAP* **03** (2019) 027 [[1811.08436](#)].
- [61] T.D.P. Edwards, M. Chianese, B.J. Kavanagh, S.M. Nissanke and C. Weniger, *Unique Multimessenger Signal of QCD Axion Dark Matter*, *Phys. Rev. Lett.* **124** (2020) 161101 [[1905.04686](#)].
- [62] J.F. Navarro, C.S. Frenk and S.D.M. White, *The Structure of cold dark matter halos*, *Astrophys. J.* **462** (1996) 563 [[astro-ph/9508025](#)].
- [63] HAWC collaboration, *Search for decaying dark matter in the Virgo cluster of galaxies with HAWC*, *Phys. Rev. D* **109** (2024) 043034 [[2309.03973](#)].
- [64] T. Lacroix, C. Boehm and J. Silk, *Ruling out thermal dark matter with a black hole induced spiky profile in the M87 galaxy*, *Phys. Rev. D* **92** (2015) 043510 [[1505.00785](#)].
- [65] P. Gondolo and J. Silk, *Dark matter annihilation at the galactic center*, *Phys. Rev. Lett.* **83** (1999) 1719 [[astro-ph/9906391](#)].
- [66] S. Balaji, D. Sachdeva, F. Sala and J. Silk, *Dark matter spikes around Sgr A* in γ -rays*, *JCAP* **08** (2023) 063 [[2303.12107](#)].
- [67] M. Phoroutan-Mehr and H.-B. Yu, *Relaxing Constraints on Dark Matter Annihilation Near the Supermassive Black Hole in M87*, [2411.18751](#).
- [68] H. Beuther, E.B. Churchwell and C.F. McKee, *The formation of massive stars*, in *Protostars and Planets V*, 2, 2006 [[astro-ph/0602012](#)].
- [69] H.L. Marshall, B.P. Miller, D.S. Davis, E.S. Perlman, M.W. Wise, C.R. Canizares et al., *A High resolution x-ray image of the jet in M87*, *Astrophys. J.* **564** (2002) 683 [[astro-ph/0109160](#)].
- [70] J.C. Tan, H. Beuther and F. Walter, *A Search for Molecular Gas in the Nucleus of M87 and Implications for the Fueling of Supermassive Black Holes*, *Astrophys. J.* **689** (2008) 775 [[astro-ph/0610488](#)].
- [71] <https://eventhorizontelescope.org/for-astronomers/data>.
- [72] M.L. Lister, H.D. Aller, M.F. Aller, M.H. Cohen, D.C. Homan, M. Kadler et al., *MOJAVE: Monitoring of Jets in Active Galactic Nuclei with VLBA Experiments. V. Multi-Epoch VLBA Images*, *The Astronomical Journal* **137** (2009) 3718 [[0812.3947](#)].
- [73] D.E. Harris, C.C. Cheung, L. Stawarz, J.A. Biretta and E.S. Perlman, *Variability Timescales in the M87 Jet: Signatures of E^2 Losses, Discovery of a Quasi Period in HST-1, and the Site of TeV Flaring*, *The Astrophysics Journal* **699** (2009) 305 [[0904.3925](#)].
- [74] A. et al, *Fermi Large Area Telescope Gamma-Ray Detection of the Radio Galaxy M87*, *The Astrophysics Journal* **707** (2009) 55 [[0910.3565](#)].
- [75] H.E.S.S. collaboration, *Discovery of very high energy gamma-rays associated with an x-ray binary*, *Science* **309** (2005) 746 [[astro-ph/0508298](#)].

- [76] V.A. Acciari et al., *Observation of gamma-ray emission from the galaxy M87 above 250 GeV with VERITAS*, *Astrophys. J.* **679** (2008) 397 [0802.1951].
- [77] MAGIC collaboration, *A lower bound on intergalactic magnetic fields from time variability of 1ES 0229+200 from MAGIC and Fermi/LAT observations*, *Astron. Astrophys.* **670** (2023) A145 [2210.03321].
- [78] D. Wadekar and Z. Wang, *Strong constraints on decay and annihilation of dark matter from heating of gas-rich dwarf galaxies*, *Phys. Rev. D* **106** (2022) 075007 [2111.08025].
- [79] C. O’Hare. <https://github.com/cajohare/AxionLimits>.
- [80] <https://asd.gsfc.nasa.gov/luvoir/>.
- [81] S.R. Kulkarni et al., *Science with the Ultraviolet Explorer (UVEX)*, 2111.15608.